International Journal of
Molecular Sciences

MDPI

Article

Synthesis of 3-(2-Alkylthio-4-chloro-5-methylbenzenesulfonyl)-2-(1-phenyl-3-arylprop-2-enylideneamino)guanidine Derivatives with Pro-Apoptotic Activity against Cancer Cells

Aneta Pogorzelska [1,*], Jarosław Sławiński [1,*], Anna Kawiak [2], Grzegorz Stasiłojć [3] and Jarosław Chojnacki [4]

[1] Department of Organic Chemistry, Medical University of Gdańsk, Al. Gen. J. Hallera 107, 80-416 Gdańsk, Poland
[2] Department of Biotechnology, Intercollegiate Faculty of Biotechnology, University of Gdańsk and Medical University of Gdańsk, Abrahama 58, 80-307 Gdańsk, Poland
[3] Department of Cell Biology and Immunology, Intercollegiate Faculty of Biotechnology of UG and MUG, Medical University of Gdańsk, Dębinki 1, 80-211 Gdańsk, Poland
[4] Department of Inorganic Chemistry, Gdańsk University of Technology, Narutowicza 11/12, 80-233 Gdańsk, Poland
* Correspondence: aneta.pogorzelska@gumed.edu.pl (A.P.); jaroslaw.slawinski@gumed.edu.pl (J.S.)

Abstract: The untypical course of reaction between chalcones and benzenesulfonylaminoguanidines led to the new 3-(2-alkylthio-4-chloro-5-methylbenzenesulfonyl)-2-(1-phenyl-3-arylprop-2-enylideneamino)guanidine derivatives **8**–**33**. The new compounds were tested in vitro for their impact on the growth of breast cancer cells MCF-7, cervical cancer cells HeLa and colon cancer cells HCT-116 by MTT assay. The results revealed that the activity of derivatives is strongly related to the presence of hydroxy group in the benzene ring at the 3-arylpropylidene fragment. The most cytotoxic compounds **20** and **24** displayed mean IC_{50} values of 12.8 and 12.7 μM, respectively, against three tested cell lines and were almost 3- and 4-fold more active toward MCF-7 and HCT-116 when compared with non-malignant HaCaT cells. Furthermore, compound **24** induced apoptosis in cancer cells and caused a decrease of mitochondrial membrane potential as well as an increase of cells in sub-G1 phase in contrast to its inactive analog **31**. The strongest activity against the most sensitive HCT-116 cell line was found for compound **30** (IC_{50} = 8 μM), which was 11-fold more effective in the growth inhibition of HCT-116 cells than those of HaCaT cells. Based on this fact, the new derivatives may be promising leading structures for the search for agents for the treatment of colon cancer.

Keywords: benzenesulfonamides; benzenesulfonylguanidines; amidrazones; anticancer activity; cytotoxicity; cell cycle flow cytometry analysis; apoptosis; membrane potential

check for updates

Citation: Pogorzelska, A.; Sławiński, J.; Kawiak, A.; Stasiłojć, G.; Chojnacki, J. Synthesis of 3-(2-Alkylthio-4-chloro-5-methylbenzenesulfonyl)-2-(1-phenyl-3-arylprop-2-enylideneamino)guanidine Derivatives with Pro-Apoptotic Activity against Cancer Cells. *Int. J. Mol. Sci.* **2023**, *24*, 4436. https://doi.org/10.3390/ijms24054436

Academic Editor: Nam Deuk Kim

Received: 22 December 2022
Revised: 13 February 2023
Accepted: 16 February 2023
Published: 23 February 2023

Copyright: © 2023 by the authors. Licensee MDPI, Basel, Switzerland. This article is an open access article distributed under the terms and conditions of the Creative Commons Attribution (CC BY) license (https://creativecommons.org/licenses/by/4.0/).

1. Introduction

Cancer is becoming a global challenge. In 2020, the number of new cases worldwide has exceeded 19 million, with the number of deaths reaching nearly 10 million. These records are expected to rise, and by 2040, the number of new cases will reach 30.2 million and the number of deaths will increase to 16.3 million [1]. Although cancer incidence is mainly related to environmental factors, mortality is primarily due to late diagnosis and a lack of effective treatments. Among the currently available methods to treat cancer, the most common is the use of small molecule drugs, which have many advantages compared to biologics, such as the pharmacokinetic properties, patient compliance, easier administration, costs, and drug storage [2].

The structures of all new small-molecule drugs approved from 2015 to 2020 for cancer treatment are characterized by polynitrogen motifs [3]. A large library of cytotoxic compounds against various types of cancer consist of amidrazone/guanidine groups as a polynitrogen motif. These structures have been found in natural anticancer alkaloids, such as crambescidines or uropocidin C [4,5]. A similar motif is present in the structure

of a lot of synthethic low molecular weight compounds with cytotoxic activity depicted in Figure 1 [6–14]. Our previous research proved that the polynitrogen fragment is an important element of benzenesulfonamides with antiproliferative activity [15–20]. The amidrazone scaffold can also be found among benzensesulfonylguanidine derivatives synthesized by our team. Previously, we reported significant cytotoxic activity against human cancer cell lines or amidrazone derivatives modified by the alkynyl scaffold [17]. These results prompted us to the design new guanidines with potential anticancer activity that will be discussed below.

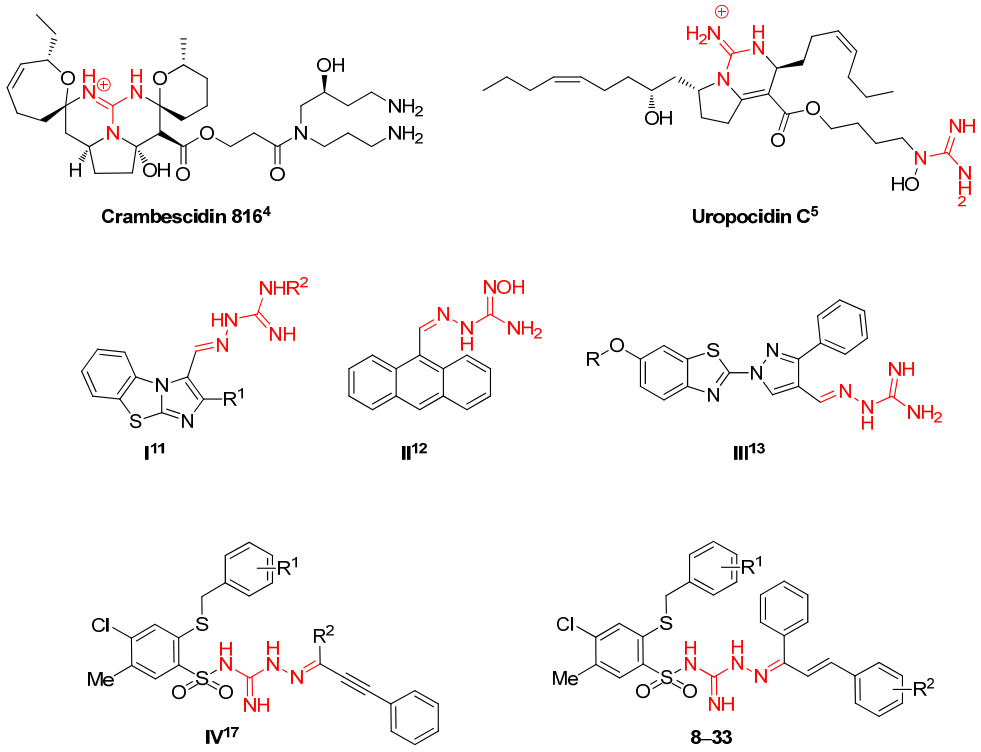

Figure 1. Some known cytotoxic compounds with the amidrazone/guanidine scaffold and the new designed derivatives **8–33**.

2. Results and Discussion

2.1. Chemistry

The synthesis of new 3-(2-alkylthio-4-chloro-5-methylbenzenesulfonyl)-2-(1-phenyl-3-arylprop-2-enylideneamino)guanidine **8–33** has been presented at Scheme 1. The appropriate substrates, 1-amino-2-(2-alkylthio-4-chloro-5-methylbenzenesulfonyl)guanidines (**1–7**), were obtained as previously described [6,21–24]. As shown, the final products **8–33** were obtained via reaction of guanidines **1–7** with a suitable chalcone derivative.

The structures of final compounds **8–33** were confirmed with spectroscopic methods IR, ^{1}H, and ^{13}C NMR, elemental analyses, and mass spectrometry.

IR spectra of compounds **8–33** showed absorption bands derived from NH bonds in the ranges 3493–3183 cm^{-1} and 1608–1653 cm^{-1}. The bands at range 1321–1342 cm^{-1} and 1125–1176 cm^{-1} were due to an SO_2 group.

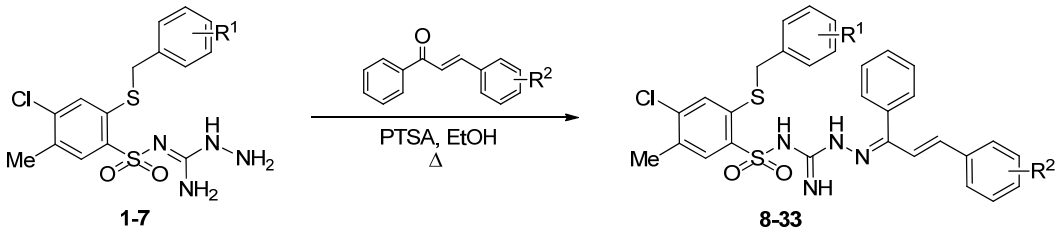

Compd	R^1	R^2
1,8	H	H
1,9	H	2-OH
1,10	H	4-OH
1,11	H	4-OMe
1,12	H	4-Cl
1,13	H	4-NO_2
2,14	2-Me	2-OH
2,15	2-Me	4-OH
3,16	3-Me	2-OH
3,17	3-Me	4-OH
4,18	4-Me	H
4,19	4-Me	2-OH
4,20	4-Me	4-OH
4,21	4-Me	4-OMe
4,22	4-Me	4-Cl
4,23	4-Me	4-NO_2
5,24	2-Cl	2-OH
5,25	2-Cl	4-OH
6,26	3-Cl	2-OH
6,27	3-Cl	4-OH
7,28	4-Cl	H
7,29	4-Cl	2-OH
7,30	4-Cl	4-OH
7,31	4-Cl	4-OMe
7,32	4-Cl	4-Cl
7,33	4-Cl	4-NO_2

Scheme 1. Synthesis of new 3-(2-alkylthio-4-chloro-5-methylbenzenesulfonyl)-2-(1-phenyl-3-arylprop-2-enylideneamino)guanidine derivatives **8**–**33**; PTSA—4-toluenesulfonic acid.

The ^{1}H NMR spectra of the series of 3-(2-alkylthio-4-chloro-5-methylbenzenesulfonyl)-2-(1-phenyl-3-arylprop-2-enylideneamino)guanidine **8**–**33** showed singlets at the range of 2.26–2.30 ppm for three protons of a methyl group. A singlet corresponding to two protons in the range of 4.21−4.33 ppm was due to a thiomethyl group. The characteristic multiplet observed in the spectra of all compounds **8**–**33** is a doublet integrated for one proton in the range of 6.20–6.60 ppm with the coupling constant $J_{H2\text{-}H3}$ = 16.1–16.6 Hz that was due to a H-2 proton (CH=C) of the double bond. The H-3 proton (C=CH) of this moiety was found at around 6.90–7.40 ppm either in multiplets or as a doublet with the corresponding coupling constant. Protons H-3 and H-6 from benzenesulfonyl scaffold appeared at the range of 7.40–7.48 ppm and 7.49–7.58 ppm, respectively. Other characteristic features of the ^{1}H NMR spectra of novel derivatives **8**–**33** are singlets with integration for 1H at chemical shift ranges 7.52–7.70 ppm, 7.66–7.82 ppm, and 9.79–10.07 ppm, which were due to NH protons.

The final confirmation of the product structure was provided by the crystallographic analysis. The data clearly indicated that the obtained products are unusual for the standard reaction between the NH-NH fragment and the chalcone derivatives. According to the literature, hydrazines react with chalcones to form pyrazoline ring [10–20]. In the case of benzenesulfonylaminoguanidines, the obtained aminoazadiene fragment does not undergo spontaneous cyclization in the standard conditions, regardless the reaction time. This was proven by X-ray diffraction studies for exampling compounds **24** and **31**.

Compound **24** forms brownish, transparent crystals satisfying symmetry of the monoclinic system, the space group $P2_1/c$ (no. 14). The asymmetric unit contains one molecule of sulfonamide and one molecule of acetone linked by hydrogen bonding. Molecular structure is shown in Figure 2. The main molecule contains a 2-chlorofenylmetyltio group disordered over two positions with site occupation factors of 0.646(6)/0.354(6). Most of the bond lengths and angles are in the expected ranges. Crystal data, data collection, and structure refinement details are summarized in S.2 (Supplementary Materials). The sulfonamide is deprotonated at N1 and the proton is transferred to N2 making N1 negatively charged and N2 positively charged (the zwitterionic form). This enables formation of strong charge-assisted hydrogen bonding in dimers present in the solid state (Figure 3). Additionally, the internal NH . . . O cyclic hydrogen bond S(6) stabilizes the conformation. The two pending hydroxyl groups bond two acetone molecules on both sides of the associate. These entities are then packed in the solid state hold by weaker Wan der Waals forces.

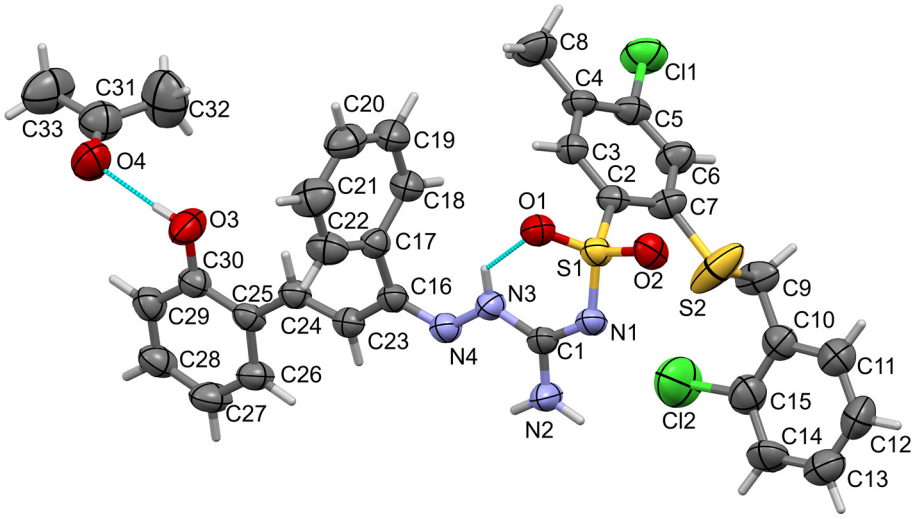

Figure 2. Molecular structure of **24** showing atom labeling scheme and hydrogen bonding shown as cyan dashed lines. Second part of disordered S2-C9-C15-Cl2 group is omitted. Displacement ellipsoids are shown at 50% probability. Selected bond lengths (Å) and angles (°): C1-N1 1.334(4), C1=N2 1.326(4), C1-N3 1.348(4), N3-N4 1.382(4), N4-C16 1.289(4), S1-N1 1.594(3), S1-C2 1.787(3), C16-C23 1.452(5), C23-C24 1.332(5), O3-C30 1.361(4), O4=C31 1.218(6), N1-S1-C2 108.44(16), C7-S2-C9 104.2(4). For parameters of hydrogen bonding see S.3 (Supplementary Materials).

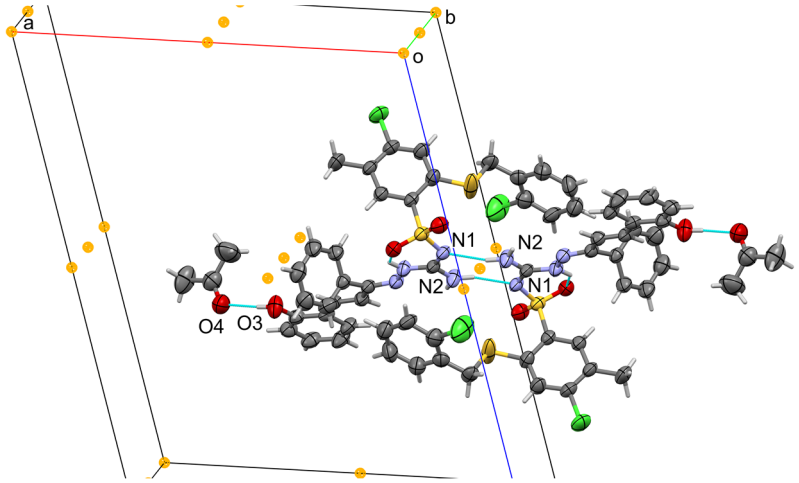

Figure 3. Crystal packing and hydrogen bonding in **24**. Molecules of the main component are linked by the ring-type hydrogen bond motif $R_2^2(8)$ NH ... N (using N1 and N2 atoms) located at the inversion center (drawn as the orange balls, screw axes, and glide planes not shown). The two acetone molecules are interacting with the sulfonamides through OH..O hydrogen bonds on both sides.

Compound **31** forms light-brown, transparent crystals satisfying the symmetry of the triclinic system, the space group $P\overline{1}$ (no. 2). The asymmetric unit contains one molecule of the protonated sulfonamide (cation) and one tosyl anion; no solvent is present this time. Molecular structure is shown in Figure 4. The tosyl sulfonic group SO_3 is disordered over two positions with site occupation factors of 0.64(3)/0.36(3). Crystal data, data collection, and structure refinement details are summarized in S.3 (Supplementary Materials). The sulfonamide is protonated at N1 and two hydrogen atoms are attached to N2. Based on bond lengths, we can assume the single-bond character of C1-N1 and C1-N2 and the double-bond character of C1=N3, making N3 formally positively charged. Then we find the formation of strong, cyclic, charge-assisted hydrogen bonding between two cations and two anions present in the solid state (Figure 5). The hydrogen bond motif can be

topologically classified as $R_4^4(16)$ or as NH ... N (using N1 and N2 as hydrogen donors and O5 and O6 from tosyl anion as acceptors) located at the inversion center (drawn as the orange ball). Additionally, the internal NH ... O cyclic hydrogen bond S(6) stabilizes the cation conformation similarly as found in **24**. These supramolecules are then packed in the solid state by other Wan der Waals forces.

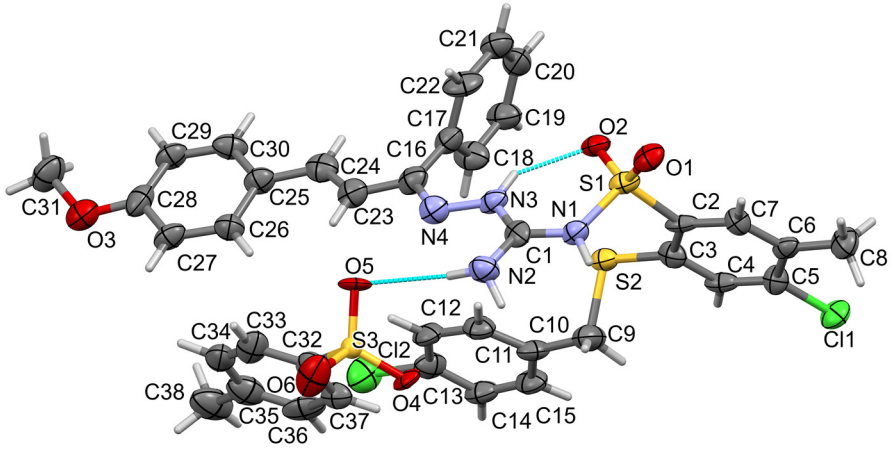

Figure 4. Molecular structure of **31** showing the atom labeling scheme and hydrogen bonding shown as cyan dashed lines. Second part of disordered -SO_3- groups is omitted. Displacement ellipsoids are shown at 50% probability. Selected bond lengths (Å) and angles (°): S1-N1 1.655(12), S1-C2 1.771(14), C1-N1 1.339(19), C1-N2 1.338(19), N3-N4 1.392(19), C1=N3 1.29(2), N4-C16 1.32(2), C23-C24 1.32(2), N1-S1-C2 105.0(6), C3-S2-C9 100.8(8).

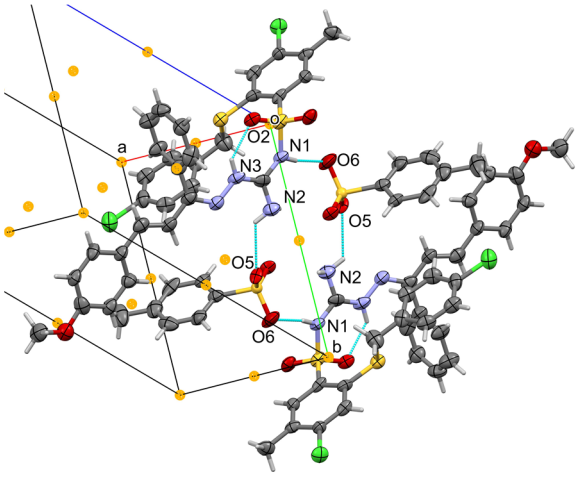

Figure 5. Crystal packing and hydrogen bonding in 31. Four ions are linked by the ring-type hydrogen bond motif $R_4^4(16)$ NH ... N (using N1 and N2 as donors and O5 and O6 from tosyl anion as acceptors) located at the inversion center (drawn as the orange ball). Again, also an internal NH ... O cycle S(6) is formed in sulfonamides (compare S.3 Supplementary Materials).

2.2. Cytotoxic Activity

The cytotoxic activity of the compounds **8**–**33** has been evaluated in MTT assays against three human cancer cell lines MCF-7 (breast cancer), HeLa (cervical cancer), and HCT-116 (colon cancer) and it was expressed as IC_{50} values in μM (Table 1).

Table 1. IC_{50} values for compounds **8**–**33** determinated after 72 h.

Compd	R^1	R^2	IC_{50} [μM]			
			MCF-7	HeLa	HCT-116	HaCaT
8	H	H	130 ± 8	120 ± 8	167 ± 7	-
9	H	2-OH	18 ± 1	17 ± 1	11 ± 0.5	35 ± 1
10	H	4-OH	15 ± 1	15 ± 1	9 ± 0.1	31 ± 1
11	H	4-OMe	330 ± 17	nd	300 ± 21	-
12	H	4-Cl	210 ± 13	190 ± 10	113 ± 6	-
13	H	4-NO_2	370 ± 20	340 ± 31	320 ± 10	-
14	2-MeC_6H_4	2-OH	13 ± 0.6	18 ± 1	9 ± 0.1	31 ± 2
15	2-MeC_6H_4	4-OH	13 ± 0.4	18 ± 0.5	10 ± 0.6	33 ± 2
16	3-MeC_6H_4	2-OH	20 ± 0.5	36 ± 2	17 ± 0.1	41 ± 2
17	3-MeC_6H_4	4-OH	17 ± 1	21 ± 1	12 ± 0.6	35 ± 2
18	4-MeC_6H_4	H	260 ± 15	200 ± 10	160 ± 5	-
19	4-MeC_6H_4	2-OH	14 ± 1	23 ± 1	11 ± 0.2	36 ± 2
20	4-MeC_6H_4	4-OH	15 ± 1	15 ± 1	8.5 ± 0.2	31 ± 1
21	4-MeC_6H_4	4-OMe	150 ± 10	250 ± 12	235 ± 5	-
22	4-MeC_6H_4	4-Cl	193 ± 10	705 ± 35	183 ± 13	-
23	4-MeC_6H_4	4-NO_2	280 ± 17	170 ± 10	nd	-
24	2-ClC_6H_4	2-OH	12 ± 0.6	17 ± 0.5	9 ± 0.5	33 ± 2
25	2-ClC_6H_4	4-OH	19 ± 1	18 ± 0.5	15 ± 0.6	41 ± 2
26	3-ClC_6H_4	2-OH	13 ± 0.6	19 ± 0.5	10 ± 0.4	38 ± 2
27	3-ClC_6H_4	4-OH	16 ± 1	20 ± 0.5	12 ± 0.1	37 ± 2
28	4-ClC_6H_4	H	230 ± 12	20 ± 1	220 ± 11	99 ± 3
29	4-ClC_6H_4	2-OH	19 ± 1	41 ± 2	18 ± 0.4	45 ± 3
30	4-ClC_6H_4	4-OH	18 ± 1	37 ± 1	8 ± 0.2	85 ± 2
31	4-ClC_6H_4	4-OMe	230 ± 13	110 ± 5	365 ± 11	-
32	4-ClC_6H_4	4-Cl	198 ± 10	nd	204 ± 12	-
33	4-ClC_6H_4	4-NO_2	220 ± 12	110 ± 3	450 ± 27	-
Cisplatin			3.0 ± 0.1	2.2 ± 0.1	3.8 ± 0.2	7.7 ± 0.2

The results indicated that cytotoxic activity is observed only for compounds with a hydroxyl group as an R^2 substituent. Compounds **20** and **24** displayed the best cytotoxic properties with mean IC_{50} values of 12.8 and 12.7 μM, respectively, against three tested cell lines. Derivatives **10**, **14**, **15**, **20**, **24**, **26**, and **30** inhibited the growth of HCT-116 cells with IC_{50} values in the range of 8–10 μM. Although the highest activity of the compounds with hydroxyl groups as the R^2 residue was against colon cancer cells, the inhibition of the growth of breast cancer cells was also remarkable. All compounds with R^2 = OH showed IC_{50} in the range of 12–20 μM against the MCF-7 cell line, and derivatives **14**, **15**, **24**, and **26** were the most promising (IC_{50} = 12 μM for **24** and 13 μM for **14**, **15**, and **26**).

The important feature of new cytotoxic agents is their selective activity against cancer cells with a weak impact on the physiology of healthy cells. Determination of the selectivity of compounds **14**–**19** and **24**–**29** was done by MTT assay with the non-cancerous HaCaT cell line (Table 2). The obtained data indicate that in the majority, compounds show significantly higher activity against cancer cells, especially HCT-116, in comparison with HaCaT cells. What is important is that the cytotoxicity against non-cancerous cells of synthesized derivatives was also significantly lower than the reference drug, cisplatin (Table 1). Compounds **20** and **24** with the best cytotoxic profile displayed also remarkable selectivity toward cancer cells in comparison with non-cancerous HaCaT cells, with a selectivity ratio nearly three and four times higher for MCF-7 and HCT-116, respectively. A similar effect was observed also for compound **26**. Importantly, the mean IC_{50} value for compound **20** and **24** against cancer cells (12.8 μM and 12.7 μM) was also significantly lower than the IC_{50} for HaCaT (31 μM and 33 μM, respectively; selectivity ratio 2.42 and 2.6, respectively). Importantly, compound **30** displayed the highest selectivity inhibiting the growth of MCF-7 and HCT-116 cells almost 5 and 11 times better, respectively, than the non-malignant cells. Importantly, the selectivity of derivative **30** was significantly better when compared to cisplatin (Table 2, selectivity index 2.56 for MCF-7 and 2.02 for HCT-116). Due to the excellent selectivity of compound **30** towards HCT-116 cells and at the same time high cytotoxicity towards this cell line (IC_{50} = 8 μM); derivative **30** may be a good hit compound for the search for chemotherapeutic agents for the treatment of colon cancer.

Table 2. The selectivity of the selected compounds **8**–**33** toward cancer cells.

Compd	R^1	R^2	Selectivity Index		
			MCF-7/HaCaT	HeLa/HaCaT	HCT-116/HaCaT
9	H	2-OH	1.9	2.1	3.2
10	H	4-OH	2.1	2.1	3.4
14	2-MeC_6H_4	2-OH	2.4	1.7	3.4
15	2-MeC_6H_4	4-OH	2.5	1.8	3.3
16	3-MeC_6H_4	2-OH	2.0	ns	2.4
17	3-MeC_6H_4	4-OH	2.1	1.7	2.9
19	4-MeC_6H_4	2-OH	1.9	1.6	3.3
20	4-MeC_6H_4	4-OH	2.1	2.1	3.6
24	2-ClC_6H_4	2-OH	2.7	1.9	3.7
25	2-ClC_6H_4	4-OH	2.2	2.3	2.7
26	3-ClC_6H_4	2-OH	2.9	2.0	3.8
27	3-ClC_6H_4	4-OH	2.3	1.8	3.1
29	4-ClC_6H_4	2-OH	2.4	ns	2.5
30	4-ClC_6H_4	4-OH	4.7	2.3	10.6
Cisplatin			2.6	3.5	2.0

ns—not selected.

2.3. Apoptotic Activity

Agents that induce apoptosis are believed to be the most effective non-surgical treatment of cancer. Therefore, the biochemical markers, such as DNA fragmentation, loss of mitochondrial membrane potential (Δψm), and phosphatidylserine translocation, were investigated. The changes in cell morphology were also examined. The experiments were done for compound **24** with the strongest cytotoxicity as well as the inactive derivative **31**. The studies of compound **24** were performed in a concentration-dependent manner using compound concentrations of 10 μM and 25 μM. The inactive analog **31** was tested only at a higher concentration of 25 μM. The charts showing the results of the cytometric analysis are presented in Figure 6.

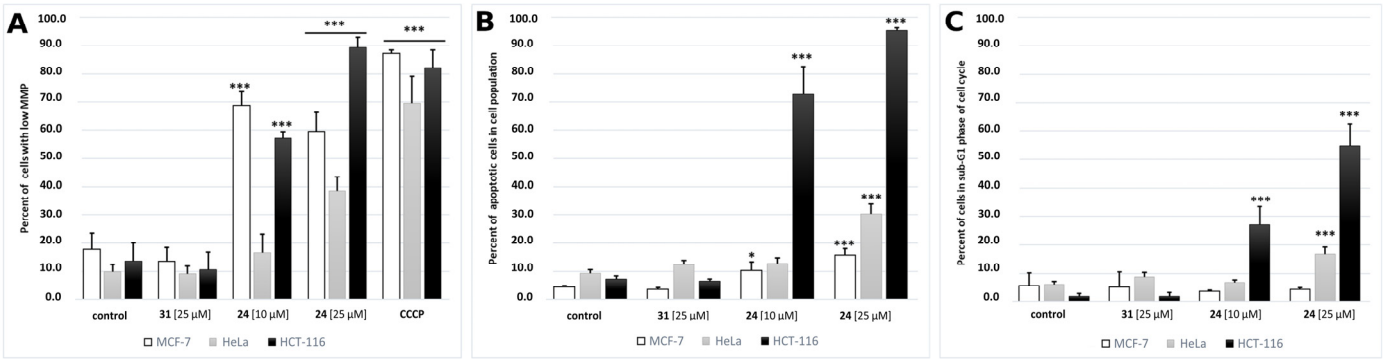

Figure 6. Cytometric analysis of MCF-7, HeLa, and HCT-116 cells treated with **24** (10 μM or 25 μM) or **31** (25 μM) for 72 h. (**A**) Mitochondrial membrane potential. MMP analysis was performed using 25 μM JC-1 staining for 30 min before the end of 72 h treatment period. As a low MMP control CCCP-treated cells (100 μM) for 15 min were used. Results represent the mean number of cells with low MMP (low JC-1 fluorescence) ± SD (n = 9) (*** $p < 0.001$). (**B**) Cytometric analysis of phosphatidylserine translocation to the outer leaflet of cell membrane. Results represent the mean number of cells with translocated phosphatidylserine ± SD (n = 9) (* $p < 0.05$; *** $p < 0.001$). Number of necrotic cells in that analysis was negligible. (**C**) Cytometric analysis of sub-G1 phase of cell cycle. Results represent the mean number of cells with translocated phosphatidylserine ± SD (n = 12) (*** $p < 0.001$).

2.3.1. Cell Morphology

The evaluation of changes in cell morphology has been performed after incubation with compounds **24** and **31** for 72 h using light microscopy. The apoptotic-like changes, such as shrinkage of the cells or detachment from the surface, were observed in the morphology of tested cells treated with both concentrations of **24** in contrast to the inactive analog **31** (Figure 7).

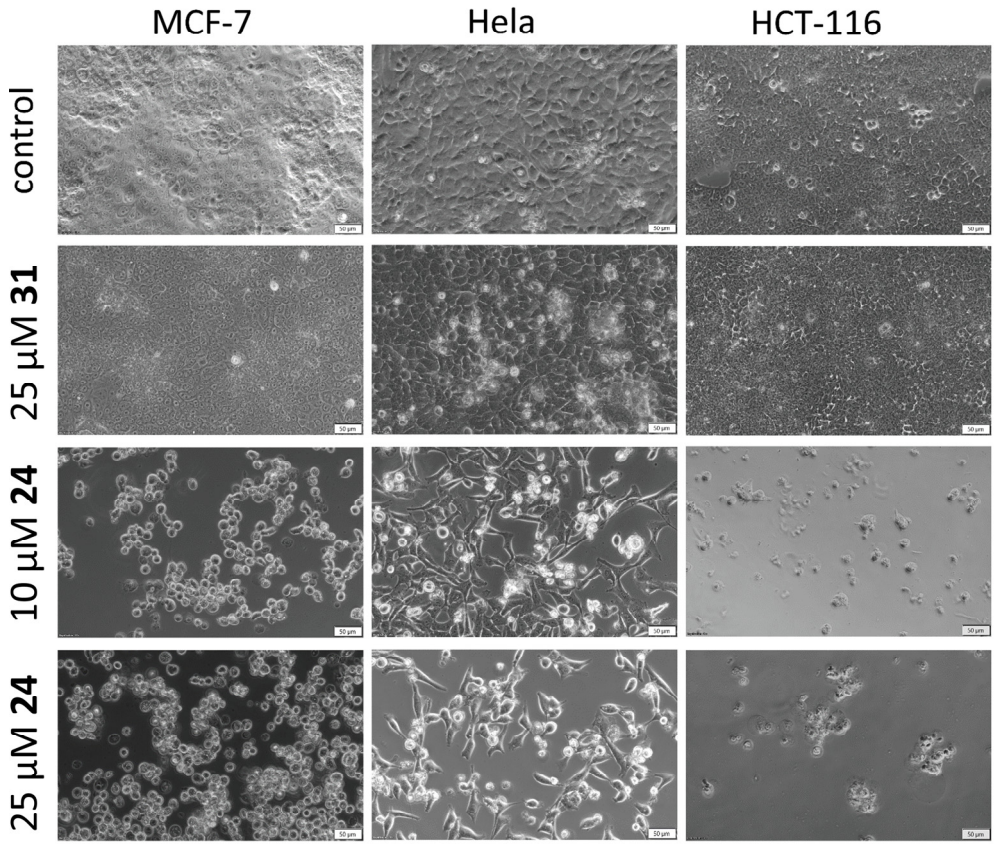

Figure 7. Morphology of MCF-7, HeLa, and HCT-116 treated with **24** or **31**. Light microscopy photographs with 20× objective of cells treated with **24** [10 μM/25 μM] or **31** [25 μM] for 72 h. Scale bar 50 μm.

2.3.2. Cell Cycle Analysis

The cell cycle distribution was measured by flow cytometry analysis after incubation of MCF-7, HeLa, and HCT-116 with compounds **24** and **31** for 72 h.

The results shown in Figure 8 indicate the significant increase in the cell distribution in the sub-G1 phase in a dose-dependent manner in the **24**-treated HCT-116 and HeLa cells (HCT-116 from 1.15% in control to 65.31%; HeLa from 5.08% in control to 18.07%). Although compound **24** affects the cell cycle of HCT-116 cells already at a concentration of 10 μM (46.69% of cells in sub-G1 phase in contrast to 1.15% in control), a slightly weaker effect is observed for HeLa cells for which a sub-G1 fraction was observed after treatment with 25 μM of **24**. In the case of MCF-7 cells treated with **24**, no significant effect on the cell cycle distribution was observed, regardless of the amidine concentration. Derivative **31**, in turn, does not substantially affect the cell cycle progression of any of the tested cell lines.

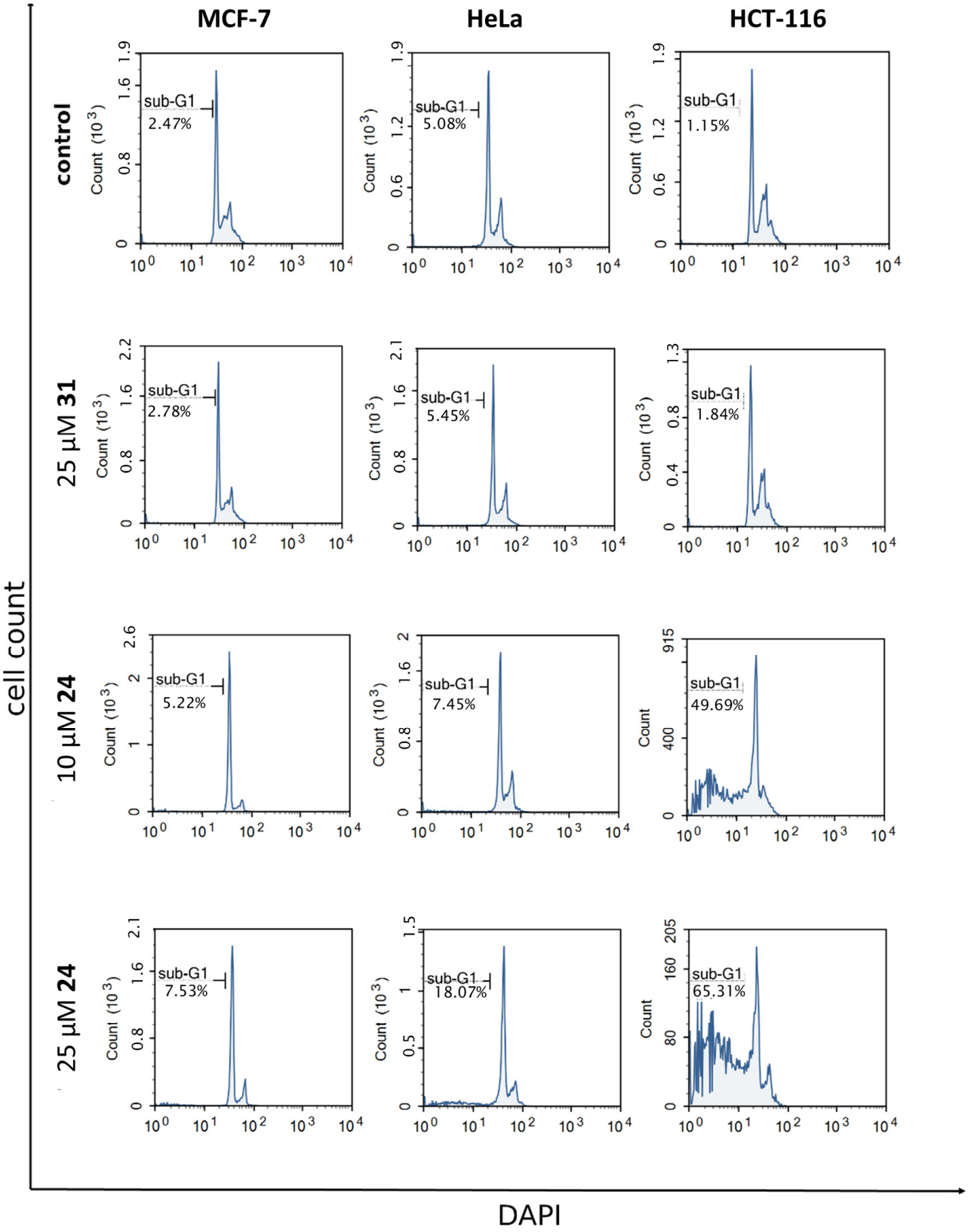

Figure 8. MCF-7, HeLa, and HCT116 cell cycle phases after 72h induction with **24** [10 μM or 25 μM] or **31** [25 μM]. On histogram, sub-G1 phase of cell cycle is visible.

2.3.3. Mitochondrial Membrane Potential ($\Delta\Psi$m) Analysis

A decrease in mitochondrial potential is one of the earliest hallmarks of apoptosis. A common method for indication of cells with high and low $\Delta\psi$m is flow cytometry combined with specific fluorescent probes, such as JC-1 (5,5′,6,6′-tetrachloro-1,1′,3,3′-tetraethylbenzimidazolylcarbocyanine iodide). JC-1 accumulates in mitochondria and forms complexes (J aggregates) with red fluorescence in healthy cells with a normal $\Delta\Psi_m$, whereas in apoptotic cells with a low $\Delta\Psi_m$ exists as a monomer with green fluorescence.

Flow cytometry analysis of MCF-7, HeLa, and HCT-116 cells treated with **24** showed a remarkable decrease in $\Delta\Psi_m$, even at a low concentration of compound, as shown in Figure 9. By contrast, exposure of cells to inactive derivative **31** did not result in a loss of $\Delta\Psi_m$.

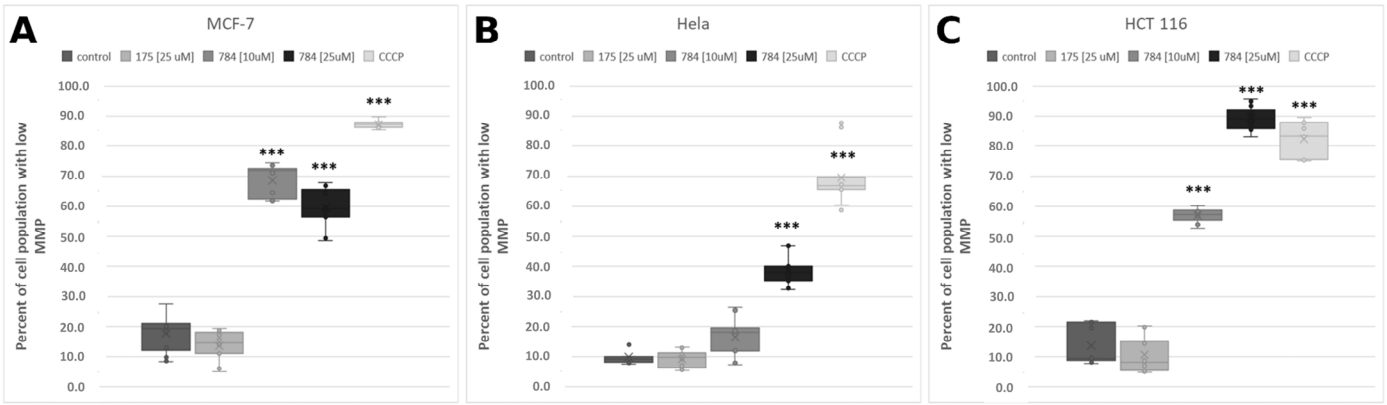

Figure 9. Changes of mitochondrial membrane potential in (**A**) MCF-7, (**B**) HeLa, and (**C**) HCT-116 cells treated with 24 (10 μM or 25 μM) or 31 (10 μM) for 72 h. MMP analysis was performed using 25 μM JC-1 staining for 30 min before the end of 72 h treatment period. As a low MMP control, 15 min CCCP-treated cells (100 μM) were used. Results represent the mean of number of cells with low MMP (low JC-1 fluorescence) ± SD (n = 9) (*** $p < 0.001$).

2.3.4. Translocation of Phosphatidylserine to Outer Leaflet of Cell Membrane

One of the early indicators of apoptosis is the exposure of phosphatidylserine residues on the cell's surface. Annexin V has a high affinity to phosphatidylserine and, as a conjugate to fluorescein isothiocyante (FITC), is widely used for detection of early apoptotic cells using flow cytometry. Detection of late-apoptotic or necrotic cells is achieved by using propidium iodide (PI) stain. Based on the obtained fluorescence, four subpopulations were found: PI-low/FITC-low (live cells), PI-high/FITC-low (necrotic cells), PI-low/FITC-high (early apoptotic cells), and PI-high/FITC-high (late apoptotic cells).

As shown in Figure 10, an increased population of apoptotic cells appeared in all tested cell lines treated with compound **24** in a dose-dependent manner. Induction of apoptosis was noticed for MCF-7 cells and HCT-116 cells exposed to **24** already at a concentration of 10 μM, and this effect was improved when exposed to a concentration of 25 μM. A significantly increased level of late apoptotic cells in the HeLa cell line was observed only after treatment with 25 μM of **24**. Importantly, incubation of cells with inactive amidine **31** did not cause statistically significant differences compared to the control.

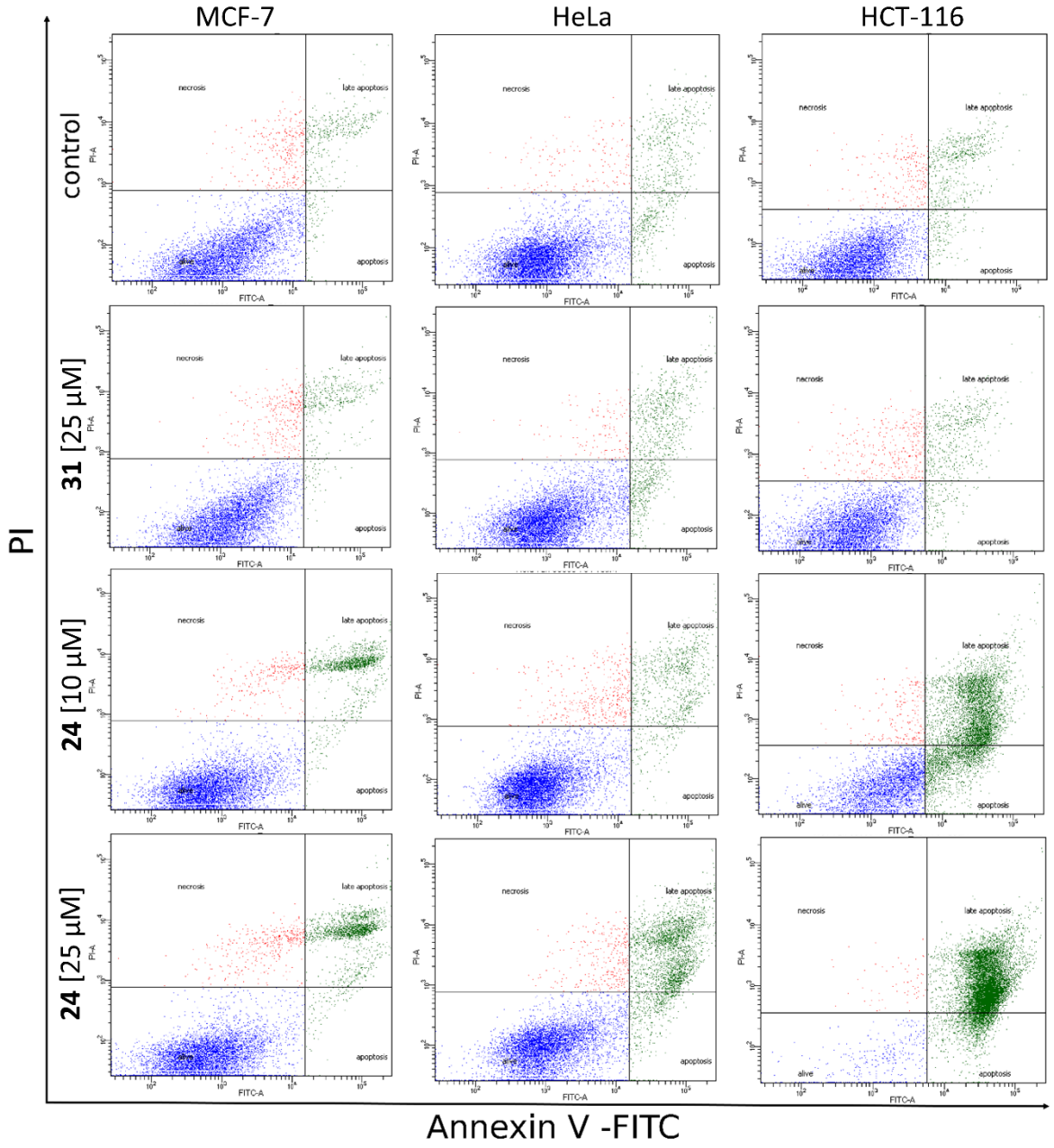

Figure 10. Features of dying process of MCF-7, HeLa, and HCT-116 cell lines. Dotblots show cells stained with Annexin V-FITC Apoptosis Kit. Cells were treated with **24** (10 µM or 25 µM) or **31** (25 µM) for 72 h. Non-treated cells were used as a control. Quadrants Q1 (upper left), Q2 (upper right), Q3 (lower left), Q4 (lower right) show the following results: necrotic cells, late apoptotic cells, alive cells, apoptotic cells, respectively.

3. Materials and Methods

3.1. Synthesis

The procedures for the preparation and spectral characteristic of compounds **8**–**33** are provided in the Supplementary Materials (S.1. Materials and methods).

3.2. Crystallographic Details

Diffraction intensity data for **24** and **31** were collected on an IPDS 2T dual beam diffractometer (STOE & Cie GmbH, Darmstadt, Germany) at 120.0(2) K with MoKa radiation of a microfocus X-ray source (GeniX 3D Mo High Flux, Xenocs, Sassenage, 50 kV, 0.6 mA, and λ = 0.71069 Å). Investigated crystals were thermostated under a nitrogen stream at 120 K

using the CryoStream-800 device (Oxford CryoSystem, Long Hanborough, Oxford, UK) during the entire experiment.

Data collection and data reduction were controlled by using the X-Area 1.75 program (STOE, 2015, Darmstadt, Germany). Numerical absorption correction was not performed due to low absorption. The structure was solved using intrinsic phasing implemented in SHELXT and refined anisotropically using the program packages Olex2 [24] and SHELX-2015 [25,26]. Positions of the C–H hydrogen atoms were calculated geometrically taking into account isotropic temperature factors. All H-atoms were refined as riding on their parent atoms with the usual restraints.

Structure **24** was refined with usual procedures; structure **31** was refined as a two-component twin, with the fraction of domains equal to 0.587(6) and 0.413(6).

Crystallographic data for all structures reported in this paper have been deposited with the Cambridge Crystallographic Data Centre as supplementary publication Nos. CCDC 2213778-2213779. The data can be obtained free of charge from The Cambridge Crystallographic Data Centre via www.ccdc.cam.ac.uk/structures (accessed on 19 Octobert 2022).

3.3. Cell Culture and Cell Viability Assay

All chemicals, if not stated otherwise, were obtained from Sigma-Aldrich (St. Louis, MO, USA). The MCF-7 cell line was purchased from Cell Lines Services (Eppelheim, Germany), the HeLa and HCT-116 cell lines were obtained from the Department of Microbiology, Tumor and Cell Biology, Karolinska Institute (Stockholm, Sweden). Cells were cultured in Dulbecco's modified Eagle's medium (DMEM) supplemented with 10% fetal bovine serum, 2 mM glutamine, 100 units/mL penicillin, and 100 µg/mL streptomycin. Cultures were maintained in a humidified atmosphere with 5% CO_2 at 37 °C in an incubator (HeraCell, Heraeus, Langenselbold, Germany).

Cell viability was determined using the MTT (3-(4,5-dimethylthiazol-2-yl)-2,5-diphenyl-tetrazoliumbromide) assay. Stock solutions of the studied compounds were prepared in 100% DMSO. Working solutions were prepared by diluting the stock solutions with DMEM medium, the final concentration of DMSO did not exceed 0.5% in the treated samples. Cells were seeded in 96-well plates at a density of 5×10^3 cells/well and treated for 72 h with the examined compounds in the concentration range 1–100 µM (1, 10, 25, 50, and 100 µM). Following treatment, MTT (0.5 mg/mL) was added to the medium and cells were further incubated for 2 h at 37 °C. Cells were lysed with DMSO and the absorbance of the formazan solution was measured at 550 nm with a plate reader (1420 multilabel counter, Victor, Jügesheim, Germany). The optical density of the formazan solution was measured at 550 nm with a plate reader (1420 multilabel counter, Victor, Jügesheim, Germany). The experiment was performed in triplicate. Values are expressed as the mean ± SD of at least three independent experiments.

3.3.1. Cell Morphology

The HeLa, MCF-7, and HCT-116 cells were seeded on 24-well plates (5×10^4/per well) in 1 mL of medium for 24 h. After that time, cells were treated with **24** and **31** for next 72 h. Cells were treated with 10 µM, 25 µM of **24,** or 25 µM of **31**. As a control, non-treated cells were used. Morphology of cells was observed after 72 h using light microscope Olympus IX83.

3.3.2. Mitochondrial Membrane Potential (Δψm) Analysis

Analyzed cells were seeded into wells of a 24-well plate at a density of 5×10^4 cells in 1000 µL, incubated overnight, and then the medium was exchanged for dilutions of reagents **24** and **31**. Before the end of 72 h of incubation, MitoProbe JC-1 (25 µM) was added into each plate well. Carbonyl cyanide m-chlorophenylhydrazone CCCP (200 nM) as the mitochondrial oxidative phosphorylation uncoupler was added into the positive control 15 min before JC-1 was added. After 30 min of JC-1 staining, cells were washed with PBS and then trypsinized (Corning® 25-053CI). Cells suspended in PBS were analyzed by flow

cytometry at λ excitation (ex) = 488 nm and λ emission (em) = 525/570 nm (LSR II BD Biosciences, San Jose, CA, USA).

3.3.3. Translocation of Phosphatidylserine to the Outer Leaflet of Cell Membrane

Analysis was performed using FITC-conjugated annexin-V (Annexin V-FITC Apoptosis Kit I, BD Biosciences, San Jose, CA, USA) according to the manufacturer's instructions (BD Biosciences) as described previously [27]. HeLa, MCF-7, and HCT-116, after seeding to 24-well plates (5×10^4/per well) and 24 h incubation, were treated for 72 h with **24** or **31** (10/25 μM or 25 μM concentration respectively). Following treatment, cells were washed in PBS, centrifuged, and then resuspended in a binding buffer. Afterward, the cells were incubated for 15 min at 37 °C with FITC-conjugated annexin-V and propidium iodide. The samples were then analyzed using a LSR II flow cytometer (BD Biosciences) using 530 ± 25 nm (Annexin V-FITC) and 575 ± 26 nm (PI).

The subpopulations were identified according to their fluorescence: PI-low/FITC-low (live cells), PI-high/FITC-low (necrotic cells), PI-low/FITC-high (early apoptotic cells), and PI-high/FITC-high (late apoptotic cells).

3.3.4. Statistical Analysis

Statistical differences between control and treated cells were determined using the One-Way ANOVA test followed by Dunn's post hoc test with Bonferroni corrected *p* values. The analyses were performed using 9 to 15 replicates run in at least three independent experiments. Statistical analysis was performed using PAST 4.0.

4. Conclusions

We synthesized a new series of 3-(2-alkylthio-4-chloro-5-methylbenzenesulfonyl)-2-(1-phenyl-3-arylprop-2-enylideneamino)guanidine derivatives **8**–**33,** which have been tested for their antiproliferative activity against three cancer cell lines: colon HCT-116, cervical HeLa, and breast MCF-7. The results indicated that the activity of the synthesized compounds was entirely dependent on the R^2 substituent and occurred only when R^2 = OH. The highest sensitivity to compounds witrh a hydroxy group in phenyl, substituted at position 4 of the amidrazone scaffold, was noticed for the colon cancer cell line HCT-116. HeLa and MCF-7 cells were slightly less sensitive. 3-{4-Chloro-2-[(4-methylphenyl)methylthio]-5-methylbenzenesulfonyl}-2-[3-(4-hydroxyphenyl)-1-phenylprop-2-enylideneamino]guanidine (**20**) and 3-{4-chloro-2-[(2-chlorophenyl)methylthio]-5-methylbenzenesulfonyl}-2-[3-(2-hydroxyphenyl)-1-phenylprop-2-enylideneamino]guanidine (**24**) were the compounds with the strongest cytotoxicity against tested cancer cell lines and good selectivity in comparison with their activity toward normal HaCaT cells.

The cytotoxicity of novel compounds is associated with the induction of apoptosis, especially on HCT-116 and MCF-7 cells as was shown in the studies with Annexin V and analysis of the mitochondrial membrane potential after treatment of cancer cells with compound **24** and its inactive analog **31**.

Despite the high activity of compounds **20** and **24**, the structure with the best parameters against the most sensitive HCT-116 cells was 3-{4-chloro-2-[(4-chlorophenyl)methylthio]-5-methylbenzenesulfonyl}-2-[3-(4-hydroxyphenyl)-1-phenylprop-2-enylideneamino]guanidine (**30**) with the lowest IC_{50} (8 μM) and the highest selectivity when compared to non-cancerous HaCaT cells (11 times stronger growth inhibition of HCT-116 then HaCaT). Taking into account cytotoxicity and selectivity toward HCT-116 cells, compound **30** is a good leading structure for the search of new agents for the treatment of colon cancer.

Supplementary Materials: The following supporting information can be downloaded at: https://www.mdpi.com/article/10.3390/ijms24054436/s1.

Author Contributions: A.P. and J.S. created the concept and designed the study; A.P. performed the synthesis of compounds; A.P. and J.S. wrote the manuscript; A.K. tested the cytotoxic activity toward HCT-116, MCF-7, HeLa, and HaCaT cell lines for all obtained compounds; G.S. performed studies for apoptotic activity; J.C. performed crystallographic analysis. All the authors discussed the results of the manuscript. All authors have read and agreed to the published version of the manuscript.

Funding: The APC was funded by Medical University of Gdańsk under "Excellence Initiative—Research University" program. The financial support to maintenance of research facilities used in these studies from Gdańsk University of Technology by the DEC-2/2021/IDUB/V.6/Si grant under the SILICIUM SUPPORTING CORE R&D FACILITIES—"Excellence Initiative—Research University" program is gratefully acknowledged.

Institutional Review Board Statement: Not applicable.

Informed Consent Statement: Not applicable.

Data Availability Statement: All data are available as Supplementary Materials.

Acknowledgments: The LC-MS was provided by the Laboratory of Mass Spectrometry at the Intercollegiate Faculty of Biotechnology University of Gdansk and Medical University of Gdansk. We would like to acknowledge the Mobi4Health EU project, which allowed us to use high quality mass spectrometers. Mobi4Health has received funding from the European Union's Seventh Framework Program for research, technological development, and demonstration under grant agreement No. 316094 and from the Ministry of Science and Higher Education.

Conflicts of Interest: The authors declare no conflict of interest.

References

1. International Agency for Research on Cancer. Available online: https://gco.iarc.fr/tomorrow/en/dataviz/isotype?types=0&single_unit=500000 (accessed on 27 June 2022).
2. A Few Q&As about Small Molecule Inhibitors. Available online: https://www.pharmiweb.com/article/a-few-qas-about-small-molecule-inhibitors (accessed on 27 June 2022).
3. Liang, X.; Wu, P.; Yang, Q.; Xie, Y.; He, C.; Yin, L.; Yin, Z.; Yue, G.; Zou, Y.; Li, L.; et al. An update of new small-molecule anticancer drugs approved from 2015 to 2020. *Eur. J. Med. Chem.* **2021**, *220*, 113473. [CrossRef] [PubMed]
4. Roel, M.; Rubiolo, J.A.; Guerra-Varela, J.; Silva, S.B.L.; Thomas, O.P.; Cabezas-Sainz, P.; Sánchez, L.; López, R.; Botana, L.M. Marine guanidine alkaloids crambescidins inhibit tumor growth and activate intrinsic apoptotic signaling inducing tumor regression in a colorectal carcinoma zebrafish xenograft model. *Oncotarget* **2016**, *7*, 83071–83087. [CrossRef] [PubMed]
5. Dyshlovoy, S.A.; Kudryashova, E.K.; Kaune, M.; Makarieva, T.N.; Shubina, L.K.; Busenbender, T.; Denisenko, V.A.; Popov, R.S.; Hauschild, J.; Fedorov, S.N.; et al. Urupocidin C: A new marine guanidine alkaloid which selectively kills prostate cancer cells via mitochondria targeting. *Sci. Rep.* **2020**, *10*, 9764. [CrossRef] [PubMed]
6. Habashneh, A.Y.; El-Abadelah, M.M.; Bardaweel, S.K.; Taha, M. Synthesis and Structure-Activity Relationship; Exploration of some Potent Anti-Cancer Phenyl Amidrazone Derivatives. *Med. Chem.* **2018**, *14*, 468–477. [CrossRef]
7. Abu-Aisheh, M.N.; Mustafa, M.S.; El-Abadelah, M.M.; Naffa, R.G.; Ismail, S.I.; Zihlif, M.A.; Taha, M.O.; Mubarak, M.S. Synthesis and biological activity assays of some new N1-(flavon-7-yl)amidrazone derivatives and related congeners. *Eur. J. Med. Chem.* **2012**, *54*, 65–74. [CrossRef]
8. Sabbah, D.A.; Hajjo, R.; Sweidan, K.; Zhong, H.A. An Integrative Informatics Approach to Explain the Mechanism of Action of N1-(Anthraquinon-2-yl) Amidrazones as BCR/ABL Inhibitors, Curr. Comput. *Aided-Drug Des.* **2020**, *17*, 817–830. [CrossRef]
9. Al-Qtaitat, M.A.; El-Abadelah, M.M.; Sabbah, D.A.; Bardaweel, S.; Sweidan, K.; Sabri, S.S.; Mubarak, M.S. Synthesis, characterization, and bioactivity of new bisamidrazone derivatives as possible anticancer agents. *Med. Chem. Res.* **2018**, *27*, 1419–1431. [CrossRef]
10. Qian, Y.; Zhang, H.-J.; Lv, P.-C.; Zhu, H.-L. Synthesis, molecular modeling and biological evaluation of guanidine derivatives as novel antitubulin agents. *Bioorg. Med. Chem.* **2010**, *18*, 8218–8225. [CrossRef]
11. Andreani, A.; Granaiola, M.; Leoni, A.; Locatelli, A.; Morigi, R.; Rambaldi, M.; Varoli, L.; Lannigan, D.; Smith, J.; Scudiero, D.; et al. Imidazo[2,1-b]thiazole guanylhydrazones as RSK2 inhibitors. *Eur. J. Med. Chem.* **2011**, *46*, 4311–4323. [CrossRef]
12. Basu, A.; Sinha, B.N.; Saiko, P.; Graser, G.; Szekeres, T. *N*-Hydroxy-*N*′-aminoguanidines as anti-cancer lead molecule: QSAR, synthesis and biological evaluation. *Bioorg. Med. Chem. Lett.* **2011**, *21*, 3324–3328. [CrossRef]
13. Liu, D.C.; Gao, M.J.; Huo, Q.; Ma, T.; Wang, Y.; Wu, C.Z. Design, synthesis, and apoptosis-promoting effect evaluation of novel pyrazole with benzo[d]thiazole derivatives containing aminoguanidine units. *J. Enzym. Inhib. Med. Chem.* **2019**, *34*, 829–837. [CrossRef] [PubMed]
14. Sielaff, F.; Than, M.E.; Bevec, D.; Lindberg, I.; Steinmetzer, T. New furin inhibitors based on weakly basic amidinohydrazones. *Bioorg. Med. Chem. Lett.* **2011**, *21*, 836–840. [CrossRef] [PubMed]

15. Żołnowska, B.; Sławiński, J.; Szafrański, K.; Angeli, A.; Supuran, C.T.; Kawiak, A.; Wieczór, M.; Zielińska, J.; Bączek, T.; Bartoszewska, S. Novel 2-(2-arylmethylthio-4-chloro-5-methylbenzenesulfonyl)-1-(1,3,5-triazin-2-ylamino)guanidine derivatives: Inhibition of human carbonic anhydrase cytosolic isozymes I and II and the transmembrane tumor-associated isozymes IX and XII, anticancer activity, and molecular modeling studies. *Eur. J. Med. Chem.* **2018**, *143*, 1931–1941. [PubMed]
16. Żołnowska, B.; Sławiński, J.; Pogorzelska, A.; Szafrański, K.; Kawiak, A.; Stasiłojć, G.; Belka, M.; Zielińska, J.; Bączek, T. Synthesis, QSAR studies, and metabolic stability of novel 2-alkylthio-4-chloro-N-(5-oxo-4,5-dihydro-1,2,4-triazin-3-yl)benzenesulfonamide derivatives as potential anticancer and apoptosis-inducing agents. *Chem. Biol. Drug Des.* **2017**, *90*, 380–396. [CrossRef] [PubMed]
17. Pogorzelska, A.; Sławiński, J.; Żołnowska, B.; Szafrański, K.; Kawiak, A.; Chojnacki, J.; Ulenberg, S.; Zielińska, J.; Bączek, T. Novel 2-(2-alkylthiobenzenesulfonyl)-3-(phenylprop-2-ynylideneamino)guanidine derivatives as potent anticancer agents: Synthesis, molecular structure, QSAR studies and metabolic stability. *Eur. J. Med. Chem.* **2017**, *138*, 357–370. [CrossRef] [PubMed]
18. Sławiński, J.; Szafrański, K.; Pogorzelska, A.; Żołnowska, B.; Kawiak, A.; Macur, K.; Belka, M.; Bączek, T. Novel 2-benzylthio-5-(1,3,4-oxadiazol-2-yl)benzenesulfonamides with anticancer activity: Synthesis, QSAR study, and metabolic stability. *Eur. J. Med. Chem.* **2017**, *132*, 236–248. [CrossRef] [PubMed]
19. Sławiński, J.; Brożewicz, K.; Fruziński, A.; Główka, M.L. Synthesis and antitumor activity of novel N′-(2-benzylthiobenzenesulfonyl)-1H-pyrazole-1-amidine derivatives. *Heterocycles* **2011**, *83*, 1093–1109. [CrossRef]
20. Pogorzelska, A.; Sławiński, J.; Kawiak, A.; Żołnowska, B.; Chojnacki, J.; Stasiłojć, G.; Ulenberg, S.; Szafrański, K.; Bączek, T. Synthesis, molecular structure, and metabolic stability of new series of *N′*-(2-alkylthio-4-chloro-5-methylbenzenesulfonyl)-1-(5-phenyl-1*H*-pyrazol-1-yl)amidine as potential anti-cancer agents. *Eur. J. Med. Chem.* **2018**, *155*, 670–680. [CrossRef]
21. Sławiński, J.; Bednarski, P.; Grünert, R.; Reszka, P. Syntheses of a new series of *N*-amino-*N″*-(benzenesulphonyl)guanidine derivatives with potential antitumor activity. *Polish J. Chem.* **2003**, *77*, 53–64.
22. Sławiński, J.; Pogorzelska, A.; Żołnowska, B.; Kędzia, A.; Ziółkowska-Klinkosz, M.; Kwapisz, E. Synthesis and anti-yeast evaluation of novel 2-alkylthio-4-chloro-5-methyl-*N*-[imino-(1-oxo-(1*H*)-phthalazin-2-yl)methyl]benzenesulfonamide derivatives. *Molecules* **2014**, *19*, 13704–13723. [CrossRef]
23. Żołnowska, B.; Sławiński, J.; Pogorzelska, A.; Szafrański, K.; Kawiak, A.; Stasiłojć, G.; Belka, M.; Ulenberg, S.; Bączek, T.; Chojnacki, J. Novel 5-substituted 2-(arylmethylthio)-4-chloro-*N*-(5-aryl-1,2,4-triazin-3-yl)benzenesulfonamides: Synthesis, molecular structure, anticancer activity, apoptosis-inducing activity, and metabolic stability. *Molecules* **2016**, *21*, 808. [CrossRef] [PubMed]
24. Dolomanov, O.V.; Bourhis, L.J.; Gildea, R.J.; Howard, J.A.K.; Puschmann, H. OLEX2: A Complete Structure Solution, Refinement and Analysis Program. *J. Appl. Crystallogr.* **2009**, *42*, 339–341. [CrossRef]
25. Sheldrick, G.M. *SHELXT*—Integrated space-group and crystal-structure determination. *Acta Crystallogr. A* **2015**, *71*, 3–8. [CrossRef] [PubMed]
26. Sheldrick, G.M. Crystal structure refinement with *SHELXL*. *Acta Crystaqllogr. C* **2015**, *71*, 3–8. [CrossRef]
27. Stasiłojć, G.; Pinto, S.; Wyszkowska, R.; Wejda, M.; Słomińska, E.M.; Filipska, M.; Koszałka, P.; Swierczyński, J.; O'Connor, J.E.; Bigda, J.J. U937 variant cells as a model of apoptosis without cell disintegration. *Cell. Mol. Biol. Lett.* **2013**, *18*, 249–262. [CrossRef]

Disclaimer/Publisher's Note: The statements, opinions and data contained in all publications are solely those of the individual author(s) and contributor(s) and not of MDPI and/or the editor(s). MDPI and/or the editor(s) disclaim responsibility for any injury to people or property resulting from any ideas, methods, instructions or products referred to in the content.